5-2016

Investigation and Implementation of a Lifting Line Theory to Predict Propeller Performance

Jonathan R. Eastridge
University of New Orleans

Investigation and Implementation of a Lifting Line Theory to Predict Propeller Performance

An Honors Thesis

Submitted to the Faculty of the
School of Naval Architecture and Marine Engineering of the
University of New Orleans

In Partial Fulfilment of the
Requirements for the Degree of

Bachelor of Science
in
Naval Architecture and Marine Engineering

By

Jonathan R. Eastridge

April 21, 2016

Acknowledgments

I would not have even begun this work without the help and encouragement from my thesis advisor, Dr. Brandon Taravella. Your patience, advice, and availability made it possible for me complete this thesis. Many thanks.

I would also like to thank Dr. Lothar Birk for answering my many questions in office hours and for providing numerous resources including papers, books, and advice.

Finally, I would like to express my gratitude for my family and friends who have provided encouragement and support throughout my undergraduate education. I am thankful for every step that God has allowed me to take since I moved to New Orleans.

Table of Contents

List of Figures

List of Tables

Nomenclature

Symbol	Units	Description
(x, y)	ft	chord-wise Cartesian coordinates
A_E/A_0	-	expanded area ratio
c	ft	chord length
c/R	-	chord ratio
C_{Dv}	-	viscous drag coefficient
C_L	-	lift coefficient
C_P	-	pressure coefficient
D	ft	propeller diameter
$f(x)$	ft	camber distribution
f_0	ft	maximum camber offset
f_0/c	-	camber ratio
F_i	lbf/ft	inviscid force per unit span
$F_{T,axial}$	lbf/ft	total axial force per unit span
$F_{T,tang}$	lbf/ft	total tangential force per unit span
F_v	lbf/ft	viscous drag force per unit span
G	-	non-dimensional form of circulation, Γ
i_a, i_t	-	axial and tangential induction factors
J	-	advance coefficient
K_Q	-	torque coefficient, based on rate of rotation
K_T	-	thrust coefficient, based on rate of rotation
L	lbf	lift force per unit span

n	rev/s	rate of rotation
N	-	chord-wise discretization
P	ft	propeller blade pitch
P/D	-	propeller pitch to diameter ratio
P_∞	psi	surrounding water pressure
P_a	psi	atmospheric pressure
P_v	psi	water's vaporization pressure
r	ft	radial position of blade section
$\tilde{r}$	-	transformed radial coordinate, r
r_c, r_v	ft	control point radii
r/R	-	normalized blade section radius
r_h	ft	hub radius
R	ft	propeller radius
$t(x)$	ft	thickness distribution
t_0	ft	maximum section thickness
t_0/c	-	thickness ratio
u_a, u_c, u_t	ft/s	perturbation velocities due to attack angle, camber, and thickness
$\bar{u}_a, \bar{u}_t$	1/ft	axial and tangential velocities (respectively) induced on lifting line and normalized by Γ
u_a^*, u_t^*	ft/s	axial and tangential velocities (respectively) induced on lifting line
Q	ft-lbf	propeller torque
Re	-	sectional Reynolds number

T	lbf	propeller thrust
U	ft/s	free stream velocity (equal to V_a for the purposes of this thesis)
V^*	ft/s	total inflow velocity
$v(x)$	ft/s	vertical component of velocity field of a point vortex
V_a	ft/s	advance velocity
$\tilde{x}$	ft	transformed x-coordinate
Z	-	number of propeller blades
α	rad	angle of attack
β	rad	undisturbed inflow pitch angle
β_g	rad	geometric pitch angle
β_i	rad	hydrodynamic total inflow pitch angle
β_w	rad	wake pitch angle
$\gamma(x)$	ft/s	circulation per unit chord length
Γ	ft^2/s	total sectional circulation
η_o	-	open water efficiency
ν	ft^2/s	kinematic viscosity of water
ρ	$slug/ft^3$	water density
σ	-	cavitation number
ω	rad/s	propeller angular velocity

Abstract

Numerous hydrodynamic theories may be used to predict the performance of marine propellers. The goal of this thesis is to investigate and implement a lifting line theory as a program written in FORTRAN and to test its capabilities on some Wageningen B-Series propellers. Special attention is given to the validation of the routines involved in the implementation of the theory. Difficulties were experienced in obtaining results that accurately reflect the published experimental results, and some discussion is included regarding possibilities for the sources of these errors. Also discussed are the results of other lifting line codes and their respective differences from the current implementation.

Keywords: hydrodynamics, propellers, lifting line theory, naval architecture, marine engineering

Section 1 – Introduction

1.1 Background

The delivery of thrust to a ship by a propeller is caused by the local forces and differences in pressure that are produced by the motion of the propeller itself in the surrounding water. Ideally, this is accomplished with minimal drag and rotational losses. The complexities of the flow local to the ship and its propeller contribute to the difficulty in maintaining real-world simplifications. Numerous methods and tools exist in the field of hydrodynamics which are used to predict the lift and drag of a given propeller and its characteristics, but it can be a challenge to find or construct one which allows for a practical method of implementation while providing results that are based on assumptions in agreement with reality. Some examples of these methods include two-dimensional models, such as momentum theory and lifting line methods, and three-dimensional models, such as lifting surface methods, vortex lattice methods, panel methods, and computational fluid dynamics (or CFD) analysis. Two-dimensional models are frequently used in the preliminary prediction stages because of their practicality, whereas three-dimensional models are desirable in the stages of propeller analysis for better reliability and more complete consideration of the important factors related to the production of lift and drag. However, severe time and financial costs may be added in implementing three-dimensional models especially when purchasing commercial software or CFD codes, although they often can provide a greater range of accuracy in the prediction.

The development of a two-dimensional lifting-line representation of a propeller blade incorporates some of the important and necessary factors that need to be considered when predicting lift and drag. Some examples of this include the principal blade geometry, viscous losses (by reasonable empirical corrections), and the effects of velocities induced by helical

vorticity. Other, perhaps less significant, factors are difficult to consider using the lifting line model, such as additional propeller geometry (skew, rake, hub effects, maximum camber location etc.), since it is a two-dimensional model and chiefly considers the foil-induced circulation. The overall circulation is found at a discrete set of chord sections (2-D foils) of a blade with parameters given which describe the operation environment, and a radial distribution of these sectional circulations is formed along the span-wise direction of the blade. The resulting distribution "line" forms the basis on which the lift and drag of the propeller blade in consideration can be found.

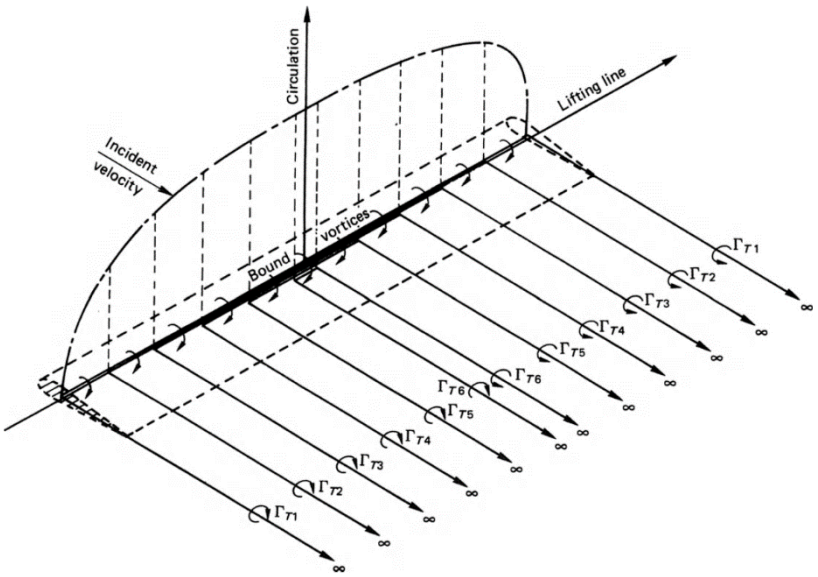

Figure 1: Illustration of Prandtl's classic lifting-line theory for a straight wing (Carlton, 2012)

1.2 Previous Work

Lifting line theory was first formally introduced in 1918 by Ludwig Prandtl and had its beginnings as a calculation of lift as a result of circulation produced by straight wings. A vortex that is said to be bound to the wing is responsible for this circulation, and it was found by Prandtl that the bound vortex strength diminishes along the span of the wing and ultimately vanishes at the wing tip. In addition to the bound vortex, a free vortex sheet (which is represented by trailing line-vortices) forms and is shed in the wake of the wing. These concepts were studied in the field

of aerodynamics and wing theory for airplanes. Numerous hydrodynamicists in the early twentieth century advanced the theory to be adapted appropriately for propellers, especially with the consideration of an infinite number of blades rotating about an origin. Further developments were made to advance the concept by formalizing the idea that realistic propellers have a finite number of blades (and thus lifting lines) instead of infinitely many lines that are so close together that they appear to form a disk. This not only brings the theory closer to reality for the calculation of circulation, but it also allows for the consideration of the influence of the vortices induced in the blades' wakes on other nearby vortex distributions. This phenomena usually causes a reduction in the delivered thrust. These vortex sheets are no longer rectangular and flat as they are in wing theory; the wake vortex sheet for propellers is helical for each blade (see Figure 2 for an illustration). Dr. H.W. Lerbs published a paper with the Society of Naval Architects and Marine Engineers (SNAME) in 1952 which gives detailed derivations of most of the components of the modern version of the theory that is implemented in this thesis. The use of Dr. Lerbs' lifting line method is quite common among naval architects to produce relatively simple and quick models of moderately-loaded propellers. Distinguishing moderately-loaded conditions from heavily loaded or lightly-loaded means that the propeller is working in the middle of its range of capabilities. As can be seen in the open water diagrams in Appendix C: Open Water Diagrams Used, the efficiency curve declines rapidly near the heavily-loaded condition and starts at zero at the lightly-loaded condition. In Dr. Lerbs' moderately-loaded model, each blade is represented by a lifting line and a

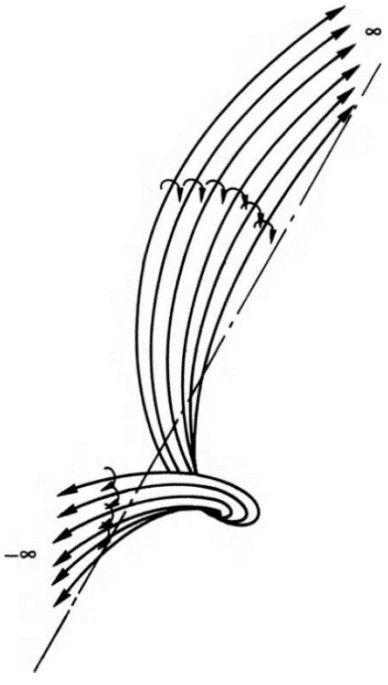

Figure 2: Helical vortex sheet (Carlton, 2012)

trailing vortex sheet which allows for an estimate to be made for the delivered thrust and torque of the propeller.

The lifting line theory's mathematical model is outlined and presented concisely by (Kerwin and Hadler, 2010). Also included is Wrench's (1957) approximations for the axial and tangential velocities induced by the helical vortex sheets as well as Glauert's method for computing the circulation produced by a two-dimensional foil section. These developments present equations which are computational-friendly and can be applied to the lifting-line method without the necessity of performing any further derivations.

1.3 Scope of this Thesis

The goal of this thesis is to implement a lifting line theory adapted to propellers in a computer program written in the FORTRAN 90 programming language. The program's versatility should allow lift and drag calculations for any propeller with a finite number of blades that has geometry which agrees reasonably with the assumptions used in the derivation of the governing equations. Programming in FORTRAN was chosen in lieu of a spreadsheet implementation for numerous reasons, some of which include the ease of operations on arrays and linear systems of equations, its power in iterative calculations, and the generation of executable files of the program code. Conveniently, lifting line theory (especially the discretization of propeller geometry which will be discussed later) requires numerous applications of iteration and the assignment of large numbers of different types of variables.

Since propeller geometry and accompanying performance data are difficult to acquire, the reliability of the program is to be tested by observing its computational methods on some Wageningen B-Series propellers and comparing the results with the existing experimental data for the corresponding performance characteristics. Though these propellers are rarely used for

implementation in modern ship applications, they are possibly the most widely used propeller series for research in propeller hydrodynamics because of their accessibility and readily available results. The Maritime Research Institute in the Netherlands (MARIN) and Dr. Gert Kuiper published *The Wageningen Propeller Series* (1992) which contains all of the necessary geometrical and performance characteristics of the Wageningen B-Series propellers to be tested in the program. The use of this propeller series and its published data will suffice in determining the reliability of the program implementation of lifting line theory. Particular attention is to be given to the details of the individual subroutines which are used for implementing the different components of lifting line theory.

Individual input files are required for each propeller to be tested containing the operating conditions and required geometry. These files are individually read into the program and separate output (results) files are automatically generated upon execution of the program. Analysis of the open water diagrams in the appendices of (Kuiper, 1992) allows for the computation of the actual performance of the propeller in consideration, and this data can then be compared to the results of the program. These "checks" are a valuable component of this thesis because the indication of the program's computational reliability will be necessary for future use and development. Therefore, three propellers with different geometries and different operating conditions will be tested.

Section 2 – The Propellers

At some point in the ship design process a propeller must be selected to meet the requirements for thrust delivery with a given applied torque. Propeller selection is no simple task due to the vast number of factors to consider. Fortunately for ship designers and hydrodynamicists, some propeller series have been developed and published with accompanying performance data given by model tests. These series can be used as a starting point for identifying the type and size of propeller that will be required to accomplish the design tasks for the ship. MARIN's B-Series has standard geometry and easily acquired data which makes it favorable for research in hydrodynamics. The available publications include experiments on over 120 models providing a various assortment of propellers with different geometrical characteristics. Further analysis with more unique propeller geometries can be accomplished upon verification of the theoretical calculations with the corresponding performance characteristics.

The geometry of the Wageningen B-Series propellers is defined in terms of the span-wise blade sections taken from the hub to the tip. Reference to (Kuiper, 1992) is sufficient for the presentation of the geometrical equations as well as the non-dimensional performance characteristics presented in the form of open-water diagrams in "Diagrams" (chapter 11). The only exception is the pitch distribution P/D – given as a ratio to the propeller's diameter – which appeared with a misprint in the 1992 publication. Reference to (Lewis, 1988) is used to obtain the correct the distribution (see Figure 3). All propellers in the B-Series have a constant pitch distribution over the radius, except for the four-bladed propellers. These have a reduction in pitch from the hub to half the radius $0.5R$. Kuiper notes that "this was done to adapt the [four-bladed] propeller[s] to the wake distribution around the hub. The effect of this pitch reduction on the propulsive parameters is negligible, however" (Kuiper, 1992, p. 41).

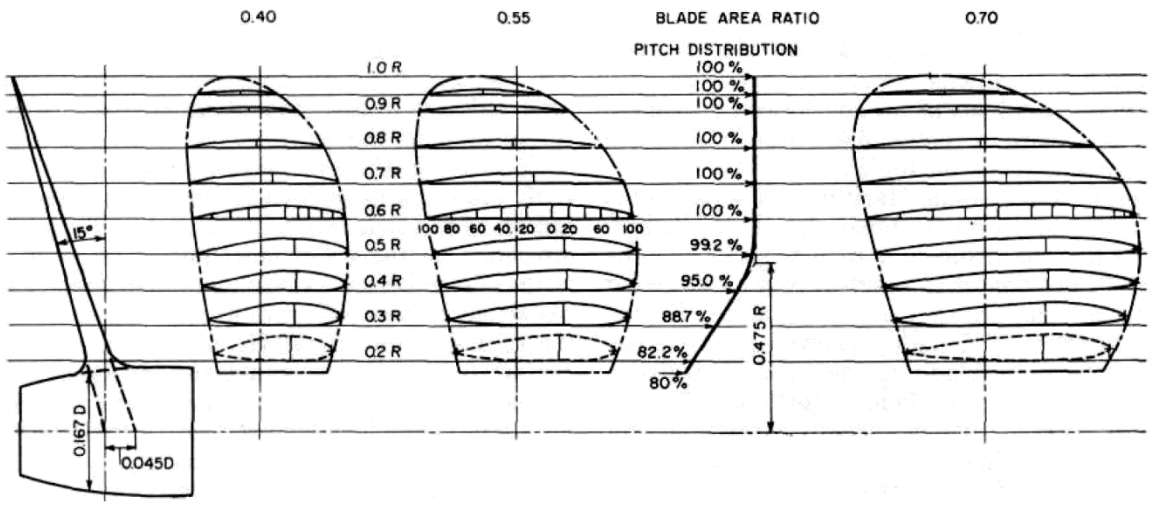

Figure 3: Pitch-diameter distribution for four-bladed B-Series Propellers (Lewis, 1988)

2.1 Geometry

Each two-dimensional foil section is defined along the radius at the appropriate distance r/R from the center of rotation and is based on various factors. The primary characteristic which determines the dimensions is the expanded area ratio A_E/A_0. Others are specific to the section of interest which makes tabulating the factors a simple method of presentation. Each characteristic is presented in non-dimensional form. The chord length is given in terms of the diameter *D*, expanded area ratio, number of blades Z, and non-dimensional factor $K(r)$. Similarly, the maximum camber f_0 is defined in terms of the maximum thickness t_0 and a factor K_f. The other necessary parameters are simply given as shown in

Table *1*. The formulas for finding the chord length and maximum camber offset are

$$c(r) = \frac{K(r) \cdot D \cdot A_E/A_0}{Z} \qquad f_0 = \frac{t_0}{2} - K_f \cdot t_0 \tag{1}$$

Of course, the geometric pitch angle is necessary and can be computed from the pitch distribution as

$$\beta_g = \tan^{-1}\left(\frac{P}{2\pi r}\right) = \tan^{-1}\left(\frac{P/R}{2\pi r/R}\right) = \tan^{-1}\left(\frac{P/D}{\pi \cdot r/R}\right) \tag{2}$$

Table 1: Factors used for determining section geometry.

			t_0/D				
r/R	*K(r)*	K_f	Z = 3	Z = 4	Z = 5	Z = 6	Z = 7
0.2	1.600	0.330	0.0406	0.0366	0.0326	0.0286	0.0246
0.3	1.832	0.271	0.0359	0.0324	0.0289	0.0254	0.0219
0.4	2.023	0.193	0.0312	0.0282	0.0252	0.0222	0.0192
0.5	2.163	0.101	0.0265	0.0240	0.0215	0.0190	0.0165
0.6	2.243	0.023	0.0218	0.0198	0.0178	0.0158	0.0138
0.7	2.247	0	0.0171	0.0156	0.0141	0.0126	0.0111
0.8	2.132	0	0.0124	0.0114	0.0104	0.0094	0.0084
0.9	1.798	0	0.0077	0.0072	0.0067	0.0062	0.0057
0.975	1.220	0	0.0042	0.0041	0.0039	0.0038	0.0037

Any particular B-Series propeller's name is formatted such that a user can easily identify the number of blades and the expanded area ratio. As an example, the B4-70 has four blades and an expanded area ratio of 0.70. Typically, once the geometry of the blade sections has been determined, a visual representation of the propeller blade is made using an expanded blade diagram (an example can be seen in Figure 4). This is a plot of the blade sections placed on their respective chord lengths at the corresponding radii.

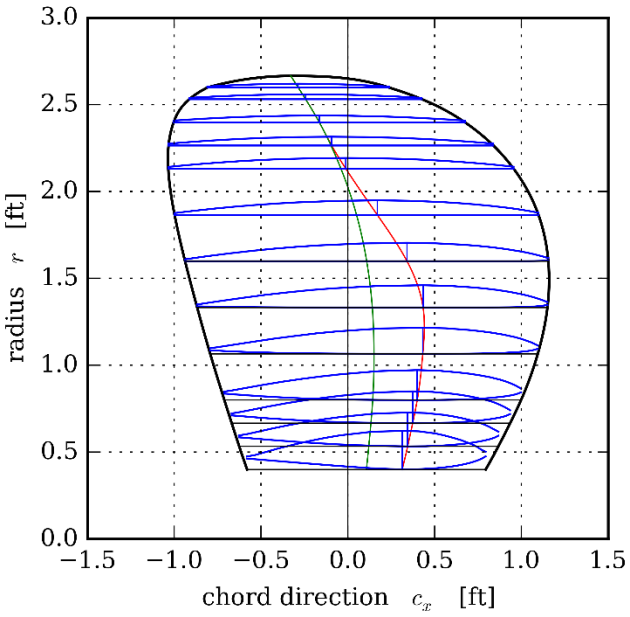

Figure 4: B4-70 Expanded blade with D = 5.33 ft (Birk, 2015)

2.2 Experimental Data: Performance Characteristics

Once a propeller with the desired geometrical characteristics has been selected, the open water diagrams generated from experimental data can be utilized to obtain the thrust and torque produced by that propeller. The curves plotted in these diagrams represent non-dimensional forms of the thrust K_T, torque K_Q (typically plotted as $10K_Q$ for clarity), and open water efficiency η_0 versus the advance coefficient J. First, the operating conditions are set to produce a selected advance coefficient. This requires iterations of the advance speed V_a and rate of rotation n (in rev/s) since J is given as

$$J = \frac{V_a}{nD} \tag{3}$$

The typical non-dimensional thrust and torque coefficients can be written in equation form as

$$K_T = \frac{T}{\rho n^2 D^4} \quad \text{and} \quad K_Q = \frac{Q}{\rho n^2 D^5} \tag{4}$$

Section 3 – Lifting Line Theory: Description of the Method

As already mentioned, the prediction of thrust and torque produced by a propeller is not a trivial task, and obtaining more realistic results requires significantly more work no matter the starting point. Lifting line theory supposedly offers moderate reliability for standard propeller geometry as a result of a moderate amount of work in the broad scope of propeller theories.

3.1 Foil Sections

The classical solution for two-dimensional foils originally given by (Glauert, 1947), which is summarized in (Kerwin and Hadler, 2010), is used by the program to compute the bound circulation produced at each chord-wise section of the propeller blade. The method assumes that the velocities induced by the local bound circulation distribution satisfy the so-called linearized boundary condition. More information can be found in (Kerwin and Hadler, 2010, pp. 15-17).

$$v(x) = U\left(\frac{\mathrm{d}f}{\mathrm{d}x} - \alpha\right) \tag{5}$$

The bound circulation is responsible for the generation of lift by each foil section of the propeller blade. Glauert's famous solution for this bound circulation distribution is based on Thin Foil Theory which assumes that the foil's thickness to chord ratio is small, or $t_0/c \ll 1$, and that the lift is produced only by the foil's camber and angle of attack (see Figure 6, top left). The foil's *mean line*, which represents the camber distribution along the chord length c of the foil section, will be used to compute the lift per unit span. An infinite series in a transformed x coordinate with coefficients related to the sectional camber distribution is used to approximate the bound circulation γ. Figure 5 is given for definition of the general use of foil coordinates.

$$\gamma(x) = -2U\left(a_0\frac{1+\cos\tilde{x}}{\sin\tilde{x}} + \sum_{n=1}^{\infty} a_n \sin(n\tilde{x})\right) \tag{6}$$

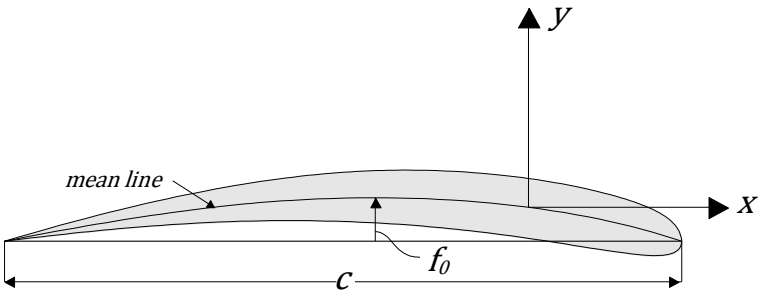

Figure 5: Foil coordinates

For a mean line which is parabolic, i.e. only the maximum camber offset f_0 and chord length c need to be defined, the camber distribution and its derivative (slope) can be expressed by

$$f(x) = f_0\left[1 - \left(\frac{x}{c/2}\right)^2\right] \tag{7}$$

$$\frac{\mathrm{d}f}{\mathrm{d}x} = -\frac{8f_0 x}{c^2} \tag{8}$$

A transformed x coordinate $\tilde{x}$ is used by Glauert and is related to x by

$$x = -\frac{c}{2}\cos\tilde{x} \tag{9}$$

which provides for easy computation of the series coefficients a_0 and a_1 as seen below.

$$\alpha - a_0 = \frac{1}{\pi}\int_0^\pi \frac{df}{dx}\mathrm{d}\tilde{x} = 0 \;\rightarrow\; a_0 = \alpha \tag{10}$$

$$a_n = \frac{2}{\pi}\int_0^\pi \frac{\mathrm{d}f}{\mathrm{d}x}\cos(n\tilde{x})\,\mathrm{d}\tilde{x} = \begin{cases} 4\dfrac{f_0}{c} & \text{for } n = 1 \\ 0 & \text{for } n > 1 \end{cases} \tag{11}$$

These simplifications allow for the infinite series to be reduced to the simple form of

$$\gamma(\tilde{x}) = -2U_\infty\alpha\left(\frac{1+\cos\tilde{x}}{\sin\tilde{x}}\right) - 8U\frac{f_0}{c}\sin\tilde{x} \tag{12}$$

The circulation distribution is integrated over the length of the chord to obtain the total sectional circulation Γ which is given by

$$\Gamma = \int_{-c/2}^{c/2}\gamma(x)\,\mathrm{d}x \tag{13}$$

The Kutta-Joukowski Lift Theorem can be used to relate this circulation strength to the lift L produced by the foil section by the simple expression

$$L = -\rho U \Gamma \tag{14}$$

Though Γ is positive counter-clockwise (for positive lift "up" in the positive y-direction) U is assumed to approach the foil in the negative x-direction, so a negative sign is introduced. In the case where the circulation is positive, or clockwise, the lift produced will be negative. Results are typically transformed into non-dimensional form for ease of computation. Lift is non-dimensionalized as the typical lift coefficient C_L which can be given for the parabolic section as

$$C_L = \frac{L}{\frac{1}{2}\rho U^2 c} = 2\pi a_0 + 4\pi \frac{f_0}{c} = 2\pi\alpha + 4\pi \frac{f_0}{c} \tag{15}$$

3.2 Perturbation Velocities and Cavitation

In order to account for more of the effects of the foil geometry, it is helpful to know more about the flow characteristics local to each foil. According to thin foil theory, the calculation of the velocity and pressure distributions very near to the foil surface is accomplished by considering only the camber, thickness, chord length, and angle of attack. First, computing the perturbation velocities – and also the pressure distribution – due to foil thickness allows for cavitation checks, so u/U is computed for a given thickness. This is done with a parabolic thickness distribution (see Figure 6, bottom).

$$t(x) = t_0 \left[1 - \left(\frac{x}{c/2}\right)^2\right] \tag{16}$$

Then, with integration as given by (Kerwin and Hadler, 2010), the disturbance velocity (normalized on U) due to thickness u_t is given as

$$\frac{u_t}{U} = -\frac{4t_0}{\pi c^2}\left[x \log\left(\frac{c/2 + x}{c/2 - x}\right) - c\right] \tag{17}$$

Other contributions to the perturbation velocity are due to the camber distribution u_c and angle of attack u_a. Their components are given respectively as

$$\frac{u_c}{U} = -\frac{1}{2}\frac{\gamma}{U} \tag{18}$$

$$\frac{u_\alpha}{U} = \alpha\sqrt{\frac{c/2 - x}{c/2 + x}} \tag{19}$$

These three components are superimposed to produce the total perturbation velocity normalized on the free stream velocity U.

$$\frac{u}{U} = \frac{u_t}{U} + \frac{u_c}{U} + \frac{u_\alpha}{U} \tag{20}$$

Still it is necessary to find the difference in the velocities on the upper and lower surfaces of the foil. The only difference is due to the circulation, so

$$\left(\frac{u}{U}\right)_{upper} = \frac{u_t}{U} - \frac{u_c}{U} + \frac{u_\alpha}{U} \quad \text{and} \quad \left(\frac{u}{U}\right)_{lower} = \frac{u_t}{U} + \frac{u_c}{U} + \frac{u_\alpha}{U} \tag{21}$$

Now the pressure coefficients on the upper and lower surfaces of the foil can be determined from the linearized Bernoulli equation (Kerwin and Hadler, 2010).

$$C_{P_{upper}} = -2\left(\frac{u}{U}\right)_{upper} \quad \text{and} \quad C_{P_{lower}} = -2\left(\frac{u}{U}\right)_{lower} \tag{22}$$

The cavitation number σ is now introduced and compared with the pressure coefficients to check for cavitation inception. If $\sigma < C_P$ then the local pressure has dropped below vaporization pressure and cavitation is likely. Here, P_∞ is the hydrostatic pressure local to the propeller shaft, P_a is the atmospheric pressure, and h is the depth of the shaft below the surface.

$$\sigma = \frac{P_\infty - P_v}{\frac{1}{2}\rho U^2} \quad \text{where} \quad P_\infty = P_a + \rho g h \tag{23}$$

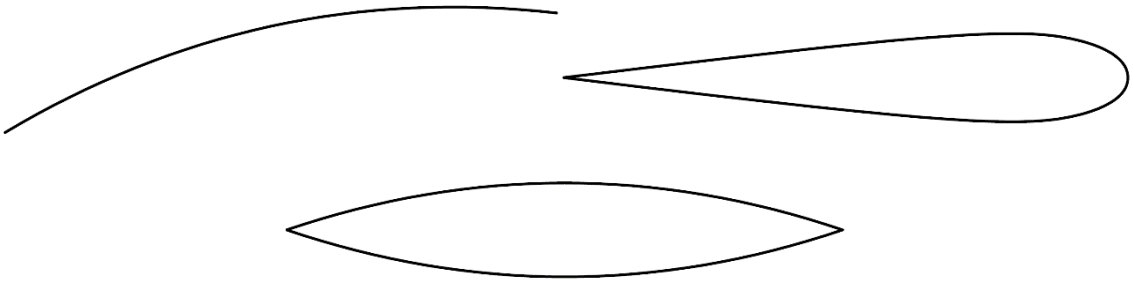

Figure 6: Foil shape approximations

Camber and angle of attack of foil section (top left), thickness of realistic foil section with no camber (top right), and foil section with symmetric parabolic thickness (bottom)

3.3 Induced Velocities

Now we are interested in approximating the velocities induced on the lifting line due to the influence of the helical vortex sheets in the wake of each blade. The computation of these induced velocities is governed by the Biot-Savart Law which was first introduced as a method of computing the magnetic flux through a point at some distance from a current-carrying wire. The Biot-Savart Law relates the magnitude, direction, and proximity of a single vortex filament in the wake of a section of the blade to the velocity at the lifting line. The vortex sheet is thought to be made up of individual line vortices shed from each foil section, and the influence of each section's wake vortex affects the velocity induced at any point on the lifting line. An analytical solution to this system practically does not exist, and evaluating the integrals numerically can be highly demanding in terms of time and effort. Fortunately, J. W. Wrench derived a set of highly accurate closed form approximations using sums of Bessel functions in 1957 (Wrench, 1957), eliminating the necessity to solve the equations numerically.

Though Wrench's equations are presented below, reference to *The Calculation of Propeller Induction Factors* (Wrench, 1957) is advised for a thorough discussion about their derivation. Essentially, $\bar{u}_a$ and $\bar{u}_t$ – the axial and tangential velocities induced by a helical vortex filament of

unit circulation strength at particular radii (each r/R) on the lifting line – are approximated using Wrench's method; then the products of these with the span-wise distribution of bound circulation (defined in section 3.5 Calculation of Thrust and Torque) are integrated over the span of the propeller blade to obtain u_a^* and u_t^* which are the total axial and tangential velocities induced at a point on the lifting line. Wrench's approximations and the velocity integrals are computed using the following equations and conditions (Kerwin and Hadler, 2010).

When $r_v > r_c$:

$$\bar{u}_a(r_c, r_v) = \frac{Z}{4\pi r_c}(y - 2Zyy_0F_1) \tag{24}$$

$$\bar{u}_t(r_c, r_v) = \frac{Z^2}{2\pi r_c} y_0 F_1 \tag{25}$$

When $r_c > r_v$:

$$\bar{u}_a(r_c, r_v) = \frac{Z^2}{2\pi r_c} yy_0 F_2 \tag{26}$$

$$\bar{u}_t(r_c, r_v) = \frac{Z}{4\pi r_c} y(1 + 2Zy_0F_2) \tag{27}$$

Where:

$$F_1 \approx \frac{-1}{2Zy_0}\left(\frac{1+{y_0}^2}{1+y^2}\right)^{0.25}\left\{\frac{U}{1-U} + \frac{1}{24Z}\left[\frac{9{y_0}^2+2}{(1+{y_0}^2)^{1.5}} + \frac{3y^2-2}{(1+y^2)^{1.5}}\right]\ln\left(1+\frac{U}{1-U}\right)\right\} \tag{28}$$

$$F_2 \approx \frac{1}{2Zy_0}\left(\frac{1+{y_0}^2}{1+y^2}\right)^{0.25}\left\{\frac{1}{U-1} - \frac{1}{24Z}\left[\frac{9{y_0}^2+2}{(1+{y_0}^2)^{1.5}} + \frac{3y^2-2}{(1+y^2)^{1.5}}\right]\ln\left(1+\frac{1}{U-1}\right)\right\} \tag{29}$$

$$U = \left[\frac{y_0\left(\sqrt{1+y^2}-1\right)}{y\left(\sqrt{1+{y_0}^2}-1\right)}\exp\left(\sqrt{1+y^2}-\sqrt{1+{y_0}^2}\right)\right]^Z \tag{30}$$

$$y = \frac{r_c}{r_v \tan\beta_w} \quad \text{and} \quad y_0 = \frac{1}{\tan\beta_w} \tag{31}$$

The Biot-Savart integrals for the induced velocities are:

$$u_a^*(r_c) = \int_{r_h}^{R} \left[-\frac{\partial \Gamma(r_v)}{\partial r} \bar{u}_a(r_c, r_v) \right] \mathrm{d}r_v \tag{32}$$

$$u_t^*(r_c) = \int_{r_h}^{R} \left[-\frac{\partial \Gamma(r_v)}{\partial r} \bar{u}_t(r_c, r_v) \right] \mathrm{d}r_v \tag{33}$$

These velocity components are essentially deductions from the undisturbed inflow velocity (see Figure 7). The control point radius r_c is the radial location on the lifting line where the velocity is induced, and the radius r_v is the radial location of the particular vortex filament of concern. Since a line vortex is shed from each of the foil's wakes, we need to compute the influence of each of these line vortices on every section. One issue experienced in the computation of these induced velocities involves the singular behavior when r_c is equal to r_v (see Figure 9). To correct this, it is "useful to factor out the singular part, leaving a regular function that depends on the geometry of the helix" (Kerwin and Hadler, 2010, pp. 80-81). This is done with the induction factors proposed by Lerbs (1952) as shown below

$$i_a(r_c, r_v) = -\frac{\bar{u}_a(r_c, r_v)}{\dfrac{1}{4\pi(r_c - r_v)}} \quad \text{and} \quad i_t(r_c, r_v) = \frac{\bar{u}_t(r_c, r_v)}{\dfrac{1}{4\pi(r_c - r_v)}} \tag{34}$$

These factors are employed in a new equation for the induced velocities as

$$u_a^* = \frac{V_a}{1 - r_h/R} \int_0^{\pi} \frac{i_a(r_c, r_v) \sum_{j=1}^{J} j a_j \cos(j\tilde{r}_v)}{\cos\tilde{r}_v - \cos\tilde{r}_c} \mathrm{d}\tilde{r}_v \tag{35}$$

$$u_t^* = \frac{-V_a}{1 - r_h/R} \int_0^{\pi} \frac{i_t(r_c, r_v) \sum_{j=1}^{J} j a_j \cos(j\tilde{r}_v)}{\cos\tilde{r}_v - \cos\tilde{r}_c} \mathrm{d}\tilde{r}_v \tag{36}$$

where a_j are the coefficients found using a Fourier transformation of the span-wise bound circulation distribution. This requires the definition of the angular coordinate $\tilde{r}$ as a transformation of the physical radial coordinate r defined by

$$\tilde{r} = \cos^{-1}\left(\frac{R + r_h - 2r}{R - r_h}\right) \tag{37}$$

The Fourier series of the circulation distribution is found in terms of the non-dimensional circulation $G(\tilde{r})$ as a function of the radial coordinate. The motivation for this is to allow the circulation to vanish at the hub and tip by using strictly a sine series. For brevity, the details of the computation of the Fourier series coefficients is omitted. Standard Fourier series analysis procedures are used (Taravella, 2015).

$$G(\tilde{r}) = \frac{\Gamma(\tilde{r})}{2\pi R V_a} = \sum_{j=1}^{J} a_j \sin(j\tilde{r}) \tag{38}$$

Using vector addition, it is clear that the total inflow velocity V^* and its angle (the hydrodynamic pitch angle) β_i from the free stream are (see Figure 7)

$$V^*(r) = \sqrt{(V_a + u_a^*)^2 + (\omega r + u_t^*)^2} \tag{39}$$

$$\beta_i = \tan^{-1}\left(\frac{V_a + u_a^*}{\omega r + u_t^*}\right) \tag{40}$$

The total inflow velocity allows for the computation of the inviscid force per unit radius as

$$F_i(r) = \rho V^*(r)\Gamma(r) \tag{41}$$

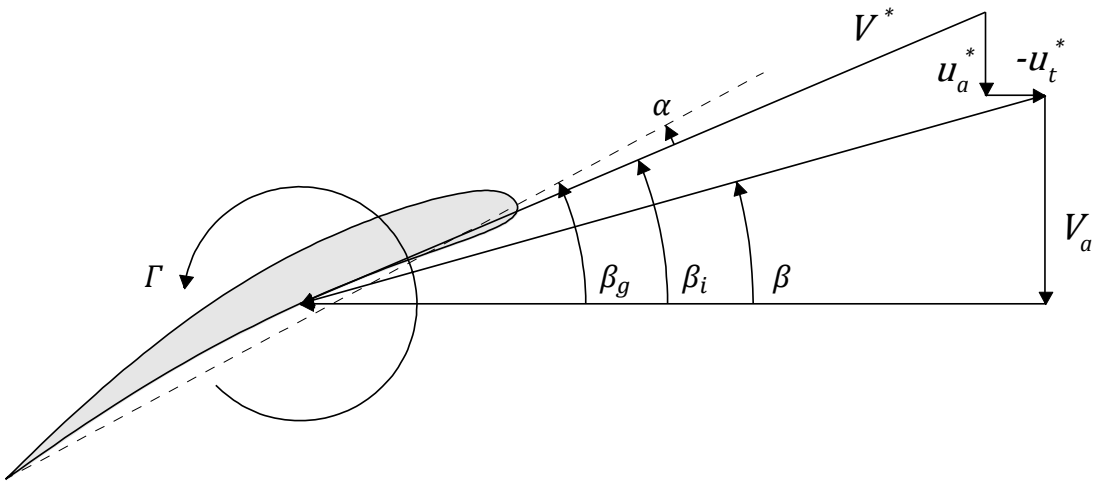

Figure 7: Foil section with velocities, angles, and circulation shown

3.4 Empirical Estimation of Viscous Drag

Since the principles of lifting line theory do not account for the viscous nature of water, it is necessary to make some correction for its effects. Fortunately, a simple method is quite sufficient using a two-dimensional flat plate drag coefficient. The coefficient of choice is the ITTC 1957 friction coefficient.

$$C_{Dv} = 2 \cdot \frac{0.075}{(\log_{10} Re - 2)^2} = \frac{0.15}{(\log_{10} Re - 2)^2} \tag{42}$$

The factor of 2 is present because propeller blades experience frictional drag on both the blade face and back. The Reynolds number found in the denominator is defined for a propeller blade section as

$$Re = \frac{cV^*}{\nu} \tag{43}$$

where ν is the kinematic viscosity of water. Then the viscous force per unit radius becomes

$$F_v(r) = \frac{1}{2}\rho[V^*(r)]^2 c(r) C_{Dv}(r) \tag{44}$$

3.5 Calculation of Thrust and Torque

Lifting line theory is given its name due to the distribution of circulation as a "lifting line" spanning the blade from the hub to the tip. The distribution of circulation may be thought of at this point as a radial distribution rather than sectional or chord-wise.

$$\gamma(r) = -\frac{\mathrm{d}\Gamma}{\mathrm{d}r} \tag{45}$$

Breaking the inviscid forces due to circulation and the viscous forces into their respective axial and tangential components provides the following for the total axial and tangential forces per unit span

$$F_{T,axial} = -\rho V^* \Gamma \cos\beta_i - \frac{1}{2}\rho (V^*)^2 c C_{Dv} \sin\beta_i \tag{46}$$

$$F_{T,tang} = -\rho V^* \Gamma \sin\beta_i - \frac{1}{2}\rho (V^*)^2 c C_{Dv} \cos\beta_i \tag{47}$$

Integrating these forces over the span of the blade and multiplying by the number of blades provides the desired torque and thrust of the propeller.

$$T = Z\int_{r_h}^{R} F_{T,axial}\,\mathrm{d}r = \rho Z \int_{r_h}^{R} \left[-V^*\Gamma\cos\beta_i - \frac{1}{2}(V^*)^2 c C_{Dv}\sin\beta_i\right]\mathrm{d}r \tag{48}$$

$$Q = Z\int_{r_h}^{R} F_{T,tang}\,\mathrm{d}r = \rho Z \int_{r_h}^{R} \left[-V^*\Gamma\sin\beta_i - \frac{1}{2}(V^*)^2 c C_{Dv}\cos\beta_i\right]\cdot r\,\mathrm{d}r \tag{49}$$

Section 4 – Program Development/Implementation

The main logical progression of the code can be observed in the main program. Subroutines are utilized to accomplish the underlying functions behind the input of information, blade discretization, velocity and circulation distribution calculations, etc. The only computations performed in the main program include the pitch angles β, β_g, β_i and angle of attack α, the total inflow speed V^*, and the thrust T and torque Q. The following subsections further explain the use of the main program and subroutines. Some particular lines of code from the program are shown to provide clarity.

4.1 The Input: Propeller Geometry and Operating Conditions

The task which must first be accomplished in the program is reading the propeller's geometry and associated operating conditions. This is accomplished by means of a subroutine called *readinfo* and is where the program receives, upon execution, the necessary information from an external document for making all of its calculations. The desired information is read from a text file (.txt) which is uniquely formatted so that the program knows where each piece of information is going to be located in the file. A sample input file can be found in Appendix B: Sample Input File. Included in the import are the propeller diameter, number of propeller blades, shaft rotational speed (rpm), advance velocity V_a, chord-wise discretization N, and number of blade sections Ns. Also included are the following one-dimensional arrays: span-wise distance of blade section (r) normalized by propeller radius (R) r/R, sectional chord length $c(r)$ to propeller radius ratio $c(r)/R$, maximum section thickness $t_0(r)$ to chord length ratio $t_0(r)/c(r)$, maximum camber offset $f_0(r)$ to chord length ratio $f_0(r)/c(r)$, and sectional geometric pitch angle $\beta_g(r)$. The number of elements in each of these arrays should match the number of blade sections for which the geometry is provided Ns. The only computations performed in the first subroutine

include converting the propeller's rotational speed to (rad/s) from (rpm) and dimensionalizing the sectional geometry, e.g. multiplying $f_0(r)/c(r)$ by $c(r)$ to obtain $f_0(r)$ in (feet).

4.2 The Main Program

As already mentioned, the main program performs only a few calculations. The first subroutine called is *readinfo* which has also already been discussed. Next, subroutines *glauert*, *thickness*, and *pressure* are called to compute the circulation and perturbation velocities at each section. Then subroutine *transforms* is called which transforms the physical radial coordinate r (dimensionalized from r/R) to $\tilde{r}$ and represents the circulation distribution as a Fourier series. Subroutine *totindvel* is then called to compute the axial and tangential induced velocities u_a^* and u_t^* at each section which are used to obtain a new inflow speed V^*, pitch angle β_i, and angle of attack α. The circulation is calculated once more using the new angle of attack, and subroutine *ittc* is called to estimate the effects of the water's viscosity using the ITTC 1957 skin friction coefficient and a Reynolds Number based on the chord length. Subroutine *transforms* is called once more for a new Fourier representation of the new circulation distribution, and finally the thrust and torque are computed using numerical integration.

4.3 Blade Section Discretization and Circulation/Lift Coefficient Calculation

The next task (after the input is received) is to perform the first iteration in the calculation of the angle of attack using the undisturbed inflow speed. This is the velocity oriented at angle β in Figure 7. The angle of attack and inflow speed allow for the calculation of the lift coefficient using subroutine *glauert* which discretizes the foil and calculates the circulation at each blade section using the classical solution for 2-D foils known as Glauert's (1947) solution. With the approximation of the foil's mean line as a parabolic mean line, the circulation distribution (normalized on the advance velocity V_a) caused by the foil's angle of attack and maximum camber

offset can be written in the code as

```
gam = -2.*alpha*((1.+dcos(xtilde))/dsin(xtilde)) - 8.*f0*dsin(xtilde)/c
```

where `xtilde` was previously defined using

```
dxtilde = pi/N
xtilde(1) = dxtilde/2.
do i = 2,N
  xtilde(i) = xtilde(i-1) + dxtilde
end do
x = -c/2.*dcos(xtilde)
```

In this subroutine, the lift coefficient is also computed using equation (14).

4.4 Foil Shape Effects and Cavitation

Since the propeller's performance prediction is dependent only upon the attack angle and camber offset of each section, it is necessary to determine the perturbation velocities due to the foil thickness and superimpose this with the disturbance velocities due to attack angle and camber for a reliable check for cavitation inception. Two subroutines are used to determine these perturbation velocities: subroutines *thickness* and *pressure*. Once again, these subroutines employ the transformed x coordinate $\tilde{x}$ and use the following lines of code for the perturbation velocities:

```
uUt = -4*t0/(pi*c**2.) * (x*dlog((c/2+x)/(c/2.-x))-c)
uUupper = uUt - gam/2. + alpha*dsqrt((c/2.-x)/(c/2.+x))
uUlower = uUt + gam/2. + alpha*dsqrt((c/2.-x)/(c/2.+x))
```

The velocity `uUt` is the disturbance velocity due to foil thickness normalized on the inflow velocity, which in this case is simply the advance velocity V_a. The superimposed equations for the total disturbance velocity are defined for the upper and lower sides of the foil as `uUupper` and `uUlower`. These velocities can then be used to obtain the pressure coefficients on the upper and lower sides of the foil as described in Section 3.2 Perturbation Velocities and Cavitation. Although this was not accomplished in the code, cavitation can now be checked for by means of the cavitation number as previously discussed.

4.5 Calculation of Velocities Induced on a Lifting Line

The velocities induced on the lifting line from the vortices shed in each of the propeller blades' helical wakes are computed using subroutines *totindvel* and *inducevel*. The latter subroutine is called within the former and is an implementation of Wrench's (1957) closed form approximations of the normalized induced velocities. Some of the equations appear in (Kerwin and Hadler, 2010) with errors that have been corrected and checked by reproducing the plots at the bottom of page 80 in (Kerwin and Hadler, 2010) in Figure 9. Subroutine *totindvel* checks each of the section's effects on all other sections and uses Lerbs' (1952) induction factors to obtain better behavior (without the inherent singularities where r_c is equal to r_v). This singular behavior (discussed in Section 3.3 Induced Velocities) at $r_c/r_v = 1$ is evident in these figures. The correction made using Lerbs' induction factors can be seen as plotted in Figure 10.

Figure 9 contains plots of the induced velocities u_a and u_t (normalized by V_a) induced on a lifting line at radius r_c/R by helical free vortices of strength $\Gamma = 2\pi R V_a$ originating at r_v = 1.0. The parameters Z = 5 and β_w = 10, 20, 30, 40, 50, and 60 degrees were set in order to recreate Kerwin's Fig. 4.20 (*Propulsion*, p. 80) for verification of subroutine *inducevel*. Velocities u_a and u_t were obtained and plotted by multiplying the normalized $\bar{u}_a$ and $\bar{u}_t$ by Γ.

A comparison of these plots with those presented by (Kerwin and Hadler, 2010) reveals no distinct differences. Therefore it may be concluded that the routines used to generate the data plotted in these figures have been validated and that the normalized induced velocities and the axial and tangential induction factors are being computed properly.

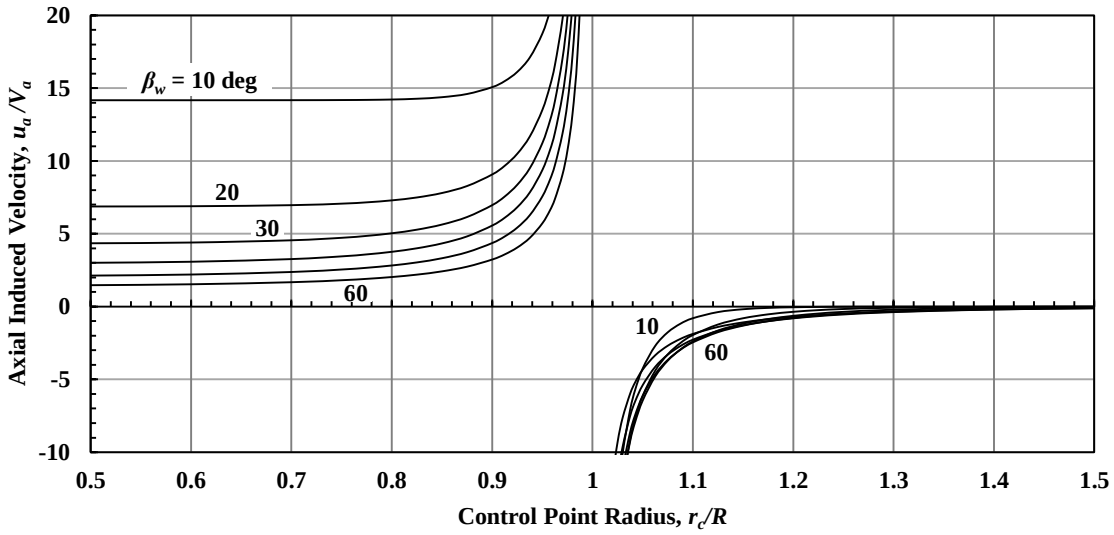

Figure 8: Normalized axial velocities induced on a lifting line

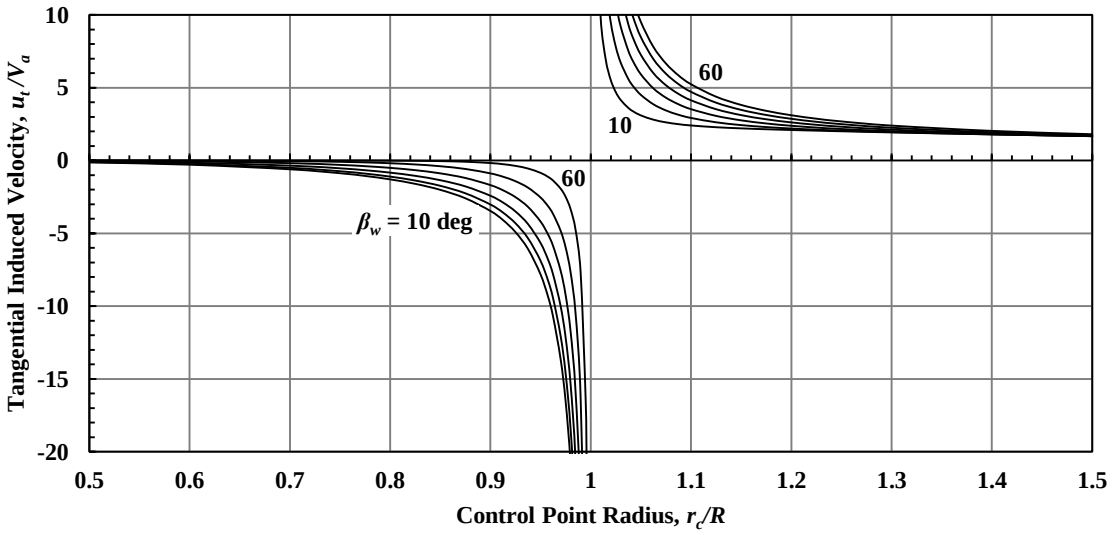

Figure 9: Normalized tangential velocities induced on a lifting line

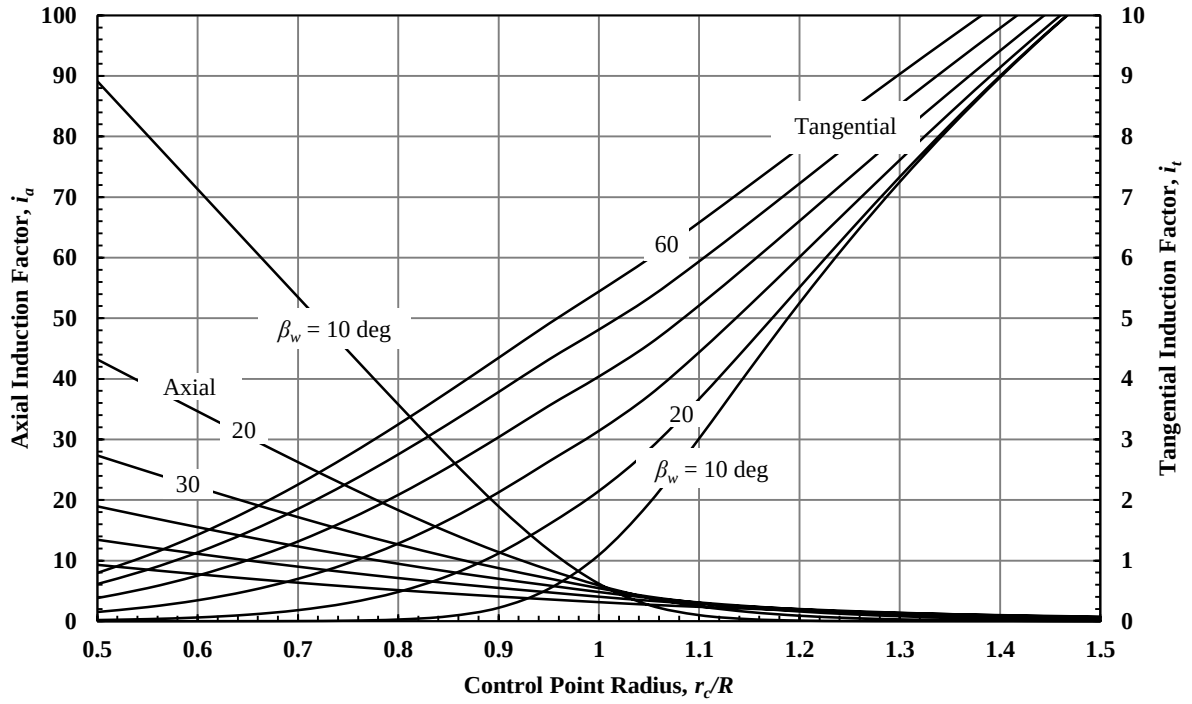

Figure 10: Lerbs induction factors for a five-bladed propeller

The code used to call subroutine *inducevel* for $\bar{u}_a$ and $\bar{u}_t$ and to compute the induction factors i_a and i_a is implemented as given below.

```
do v = 1,Ns-1

  ! Compute rv, the radii of the midpoints of rc(v) and rc(v+1)
  rv(v) = (rc(v+1)+rc(v))/2.
  drv(v) = rc(v+1)-rc(v)

  call inducevel(rc(c), rv(v), Zi, betaw, uabar(v), utbar(v))

  ! Compute Lerbs (1952) induction factors using eq. 4.56
  ia(v) = uabar(v) / (1./(4.*pi* (rc(c)-rv(v)) ))
  it(v) = utbar(v) / (1./(4.*pi* (rc(c)-rv(v)) ))

end do
```

The radial coordinate $\tilde{r}$ (at the endpoints and midpoints of the discrete spanwise circulation distribution) is computed using

```
! We need rctilde (endpoints), rvtilde (midpoints), and
! drvtilde which is the distance between endpoints
do cc = 1,Ns
  rctilde(cc) = dacos((Diam/2.+rc(1)-2.*rc(cc)) / (Diam/2.-rc(1)))
end do
```

```
do cc = 1,Ns-1
  rvtilde(cc)  = (rctilde(cc+1)+rctilde(cc))/2.
  drvtilde(cc) =  rctilde(cc+1)-rctilde(cc)
end do
```

Then the induced velocities u_a^* and u_t^* are finally computed using

```
! Compute the integrals of eq. 4.102
sumia = 0.
sumit = 0.
do v = 1,Ns-1
  sumb = 0.
  do jj = 1,J
    sumb = dble(jj)*b(jj)*dcos(dble(jj)*rvtilde(v)) + sumb
  end do
  sumia = ia(v)*sumb*drvtilde(v) / (dcos(rvtilde(v))-dcos(rctilde(c))) &
          * drvtilde(v) + sumia
  sumit = it(v)*sumb*drvtilde(v) / (dcos(rvtilde(v))-dcos(rctilde(c))) &
          * drvtilde(v) + sumit
end do

! Compute velocities ua and ut using eq. 4.102
ua =  Va / (1.-rc(1)/(Diam/2.)) * sumia
ut = -Va / (1.-rc(1)/(Diam/2.)) * sumit
```

Figure 11 shows a plot of the Fourier series representation of the non-dimensional span-wise circulation distribution for a B4-70 propeller. This was used in determining an appropriate number of Fourier coefficients to reasonably approximate the distribution. As expected, half of a sine wave is obtained for one coefficient. The fit appears to improve from two to five coefficients, but increasing the number of coefficients beyond five results in some undesirable fluctuations or "wiggles" around the actual distribution. Therefore, five coefficients were chosen for the Fourier series fit. Obviously, most of the distributions have been omitted for the sake of clarity.

The final step in the code is to compute the thrust and torque of the propeller for the given operating conditions. This is done by numerical integration of equations (47) and (48) presented in section 3.5 Calculation of Thrust and Torque. First each integrand is computed for each span-wise blade section, then a loop is utilized to add each section's contribution using a simple trapezoidal rule integration. The results are multiplied by the water density ρ (to obtain the units of lbf and ft-lbf) and the number of blades Z (to obtain the contribution from each blade on the propeller).

```
! Computing integrand of equations 4.45 and 4.46
Ti =  -V*fcirc*dcos(betai) - 0.5*(V**2.)*c*Cdv*dsin(betai)
Qi = (-V*fcirc*dsin(betai) - 0.5*(V**2.)*c*Cdv*dcos(betai))*rad


! Computing equations 4.45 and 4.46
Thrust = 0.
Torque = 0.
do cc = 2,Ns

  Thrust = 0.5*(Ti(cc)+Ti(cc-1))*(rad(cc)-rad(cc-1)) + Thrust
  Torque = 0.5*(Qi(cc)+Qi(cc-1))*(rad(cc)-rad(cc-1)) + Torque

end do
Thrust = rho*Z*Thrust
Torque = rho*Z*Torque
```

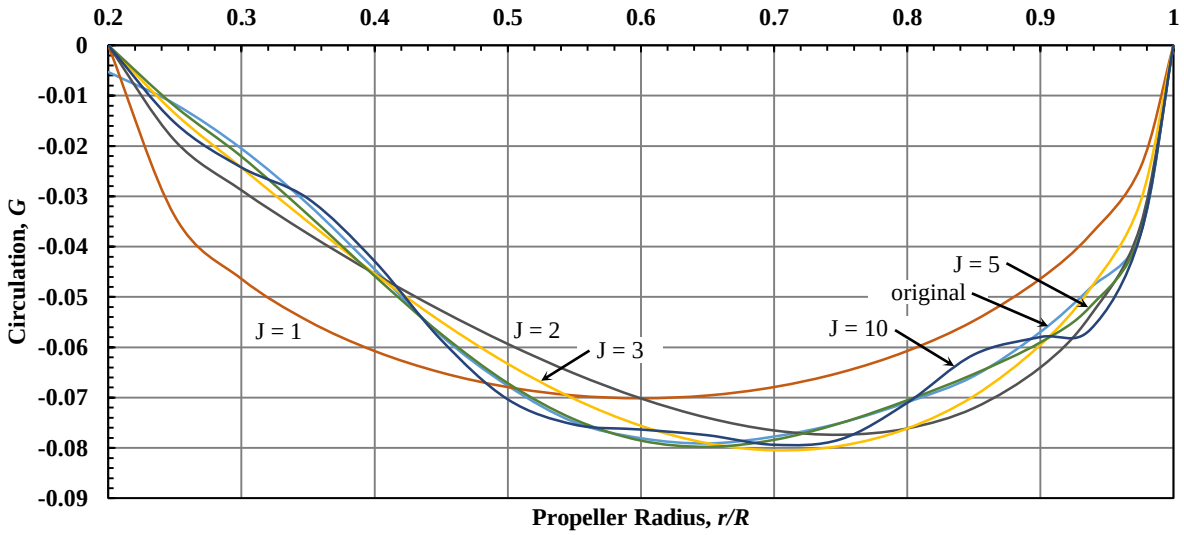

Figure 11: Fourier series representation of circulation distribution

Section 5 – Results

Typically, lifting line theory is known to yield solutions to 2-D external foil flow problems which are satisfactory in practice and principle, yet some difficulties were experienced in the development of a reliable algorithm for computing the lift generated by the rotating motion of the Wageningen B-Series propellers. The primary factors which influence the performance of the propeller according to lifting line theory are the bound and free vortices which are unique to each blade section. The bound vortex is directly related to the foil's lift coefficient at the given operating conditions and is computed using only the sectional angle of attack and camber to chord length ratio. The free vortices are the source of the induced velocities which are expected to cause a slight reduction in the produced thrust.

Table 2 shows the results of the Lifting Line code on three different propellers. Note that propeller 1 is in a "lightly loaded" operating condition while propellers 2 and 3 are considered to be in "moderately loaded" conditions. Observation of the results (see Table 3) obtained even before considering the effects of the induced velocities indicates an issue with the theory behind the bound vortex model. The source of the error is yet unknown, but suspicion lies most significantly within the validity and applicability of Glauert's solution for a 2-D thin foil to the rotating marine propeller. It is unreasonable to expect that the induced velocities will cause such a dramatic reduction in performance prediction. For example, the thrust computed for propeller 1 (see the tables below) by the program is about four times that calculated from the published experimental results (the target thrust).

Further analysis to check for convergence towards the published experimental results includes setting the maximum camber offset to zero to see the significance of its influence in the final result. A quick glance at each of the tables indicates that the blade sections' camber

influences the outcome of the prediction quite heavily, though it does not appear to be a step toward the desired solution.

Table 2: Program results

Characteristic	Symbol	Units	Propeller 1	Propeller 2	Propeller 3
Propeller diameter	D	ft	5.33	5.33	5.33
Number of blades	Z	-	4	4	3
Expanded area ratio	A_E/A_0	-	0.7	0.4	0.65
Pitch-diameter ratio	P/D	-	1.4	1.0	1.0
Advance velocity	Va	ft/s	20.0	10.0	10.0
Shaft speed	n	RPM	183.0	173.1	173.1
Propeller thrust	T	lbf	8054.2	8811.8	11252.3
Propeller torque	Q	ft-lbf	8510.1	5562.3	6354.2
Advance coefficient	J	-	1.2303	0.6503	0.6503
Thrust coefficient, calculated	K_T	-	0.5395	0.6597	0.8424
Torque coefficient, calculated	K_Q	-	0.1070	0.0781	0.0893
Thrust coefficient, target	K_T	-	0.1210	0.2000	0.1900
Torque coefficient, target	K_Q	-	0.0315	0.0340	0.0315

Table 3: Results without induced velocities

Characteristic	Symbol	Units	Propeller 1	Propeller 2	Propeller 3
Thrust coefficient, calculated	K_T	-	0.6867	0.8017	1.1293
Torque coefficient, calculated	K_Q	-	0.1326	0.0814	0.1147
Thrust coefficient, target	K_T	-	0.1210	0.2000	0.1900
Torque coefficient, target	K_Q	-	0.0315	0.0340	0.0315

Table 4: Results without camber

Characteristic	Symbol	Units	Propeller 1	Propeller 2	Propeller 3
Thrust coefficient, calculated	K_T	-	0.4005	0.5509	0.924
Torque coefficient, calculated	K_Q	-	0.0765	0.0555	0.0935
Thrust coefficient, target	K_T	-	0.1210	0.2000	0.1900
Torque coefficient, target	K_Q	-	0.0315	0.0340	0.0315

Interpolating the characteristics of the propeller blade geometry is another attempt that was made to improve the results. It was found that adding four sections at r/R = 0.25, 0.35, 0.85, and 0.9375 by means of a second-order Lagrangian polynomial (Rao, 2006) and a fifth section at the

blade tip (r/R = 1.0) with dimensions of approximately zero actually reduced the computed thrust and torque by about five percent. This is likely due to the inherent errors present in the numerical integration of the discrete data points. Adding more sections at r/R = 0.45, 0.55, 0.65, and 0.75 produced another gradual decrease in the computed performance, though the results converged rapidly.

Every computation made in the FORTRAN program was checked by hand for mistakes, and a rigorous search for mishandled sign conventions was conducted in order to identify issues with the current model of the physics of the flows. And though numerous adjustments were made as unnoticed mistakes were uncovered, a satisfactory solution was not achieved. Perhaps a different model for computing the local bound vortex distribution that is more appropriate for marine propellers could be used. Other such methods may include propeller vortex lattice methods (PVL) or panel methods which are described in detail in numerous sources. The application of Glauert's solution to the 2-D foil assumes a small thickness to chord length ratio and a high aspect ratio (i.e. a small expanded area ratio). The latter is obviously not valid for most marine propellers since cavitation is a greater threat with low expanded area ratios.

Table 5, Table 6, and Table 7 are shown to demonstrate some of the computations required in lifting line theory. The induced velocities at each section, the attack angles, lift coefficients, viscous drag coefficients, circulation distributions, and hydrodynamic inflow velocities and angles are shown. Note that the attack angles presented are those which were computed after the induced velocities have been determined. Also, $\Gamma(r)$ refers to the first computed radial circulation distribution, and $\Gamma_2(r)$ refers to the distribution found after the new attack angles have been computed.

Table 5: Propeller 1, computed characteristics

r/R	$\Gamma(r)$	u_a^*	u_t^*	V^*	β_i	α	C_L	C_{Dv}	$\Gamma_2(r)$
(ft)	(ft^2/s)	(ft/s)	(ft/s)	(ft/s)	(rad)	(rad)	(-)	(-)	(ft^2/s)
0.2	-1.776	-4.242	-5.622	16.413	1.287	-0.216	-1.079	0.008	13.216
0.25	-3.904	0.495	1.646	25.056	0.958	0.032	0.486	0.007	-9.780
0.3	-6.868	0.361	1.423	26.361	0.883	0.039	0.536	0.007	-12.072
0.35	-10.564	0.002	0.886	27.424	0.817	0.046	0.588	0.007	-14.531
0.4	-14.891	0.341	1.109	29.625	0.757	0.057	0.665	0.007	-18.582
0.45	-19.315	0.998	1.531	32.277	0.708	0.059	0.689	0.007	-22.033
0.5	-22.646	1.452	1.694	34.664	0.667	0.057	0.674	0.007	-23.576
0.55	-25.072	1.541	1.556	36.645	0.628	0.053	0.644	0.006	-24.359
0.6	-26.141	1.491	1.343	38.535	0.592	0.047	0.599	0.006	-24.149
0.65	-26.492	1.624	1.270	40.688	0.560	0.041	0.537	0.006	-22.952
0.7	-26.034	2.016	1.350	43.141	0.536	0.031	0.446	0.006	-20.175
0.75	-25.127	2.356	1.394	45.560	0.513	0.023	0.365	0.006	-17.143
0.8	-23.749	2.243	1.213	47.588	0.486	0.022	0.329	0.006	-15.586
0.85	-22.011	1.892	0.945	49.464	0.458	0.024	0.319	0.006	-14.922
0.9	-19.076	2.730	1.239	52.391	0.449	0.011	0.213	0.006	-9.348
0.9375	-16.146	4.859	2.089	55.811	0.462	-0.018	0.018	0.006	-0.713
0.975	-12.613	5.446	2.308	57.984	0.454	-0.026	-0.042	0.007	1.375
1	0.000	-19.576	-8.219	42.854	0.010	0.409	2.572	0.017	0.000

Table 6: Propeller 2, computed characteristics

r/R	$\Gamma(r)$	u_a^*	u_t^*	V^*	β_i	α	C_L	C_{Dv}	$\Gamma_2(r)$
(ft)	(ft^2/s)	(ft/s)	(ft/s)	(ft/s)	(rad)	(rad)	(-)	(-)	(ft^2/s)
0.2	-7.202	-21.587	-13.877	12.330	1.222	-0.304	-1.420	0.010	7.464
0.25	-9.728	4.243	5.981	23.000	0.668	0.160	1.502	0.008	-15.844
0.3	-12.536	1.579	3.970	21.793	0.560	0.195	1.734	0.008	-18.447
0.35	-15.579	0.034	2.682	22.010	0.473	0.223	1.921	0.008	-21.782
0.4	-18.820	0.842	2.779	24.619	0.456	0.191	1.740	0.008	-23.088
0.45	-21.877	1.988	2.965	27.458	0.452	0.151	1.504	0.008	-23.110
0.5	-24.552	2.476	2.821	29.721	0.433	0.130	1.374	0.007	-23.534
0.55	-26.476	2.463	2.503	31.631	0.405	0.120	1.300	0.007	-24.229
0.6	-27.610	2.521	2.254	33.655	0.381	0.107	1.199	0.007	-24.115
0.65	-27.871	2.965	2.164	35.981	0.369	0.087	1.029	0.007	-22.238
0.7	-27.688	3.593	2.140	38.440	0.361	0.065	0.847	0.007	-19.490
0.75	-26.869	3.891	2.030	40.705	0.348	0.053	0.721	0.007	-17.233
0.8	-25.503	3.595	1.781	42.653	0.324	0.054	0.677	0.007	-16.409
0.85	-23.756	3.279	1.563	44.645	0.302	0.056	0.644	0.007	-15.528
0.9	-20.674	4.353	1.704	47.406	0.308	0.032	0.455	0.007	-10.334
0.9375	-17.541	6.356	2.092	50.125	0.332	-0.005	0.196	0.007	-4.043
0.975	-13.727	6.652	2.146	51.985	0.326	-0.011	0.143	0.007	-2.409
1	0.000	-20.499	-4.266	45.276	-0.234	0.542	3.407	0.017	0.000

Table 7: Propeller 3, computed characteristics

r/R	$\Gamma(r)$	u_a^*	u_t^*	V^*	β_i	α	C_L	C_{Dv}	$\Gamma_2(r)$
(ft)	(ft^2/s)	(ft/s)	(ft/s)	(ft/s)	(rad)	(rad)	(-)	(-)	(ft^2/s)
0.2	-19.939	-54.137	-40.618	53.910	0.959	0.051	0.568	0.006	-28.314
0.25	-24.866	13.151	15.350	35.892	0.701	0.204	1.536	0.007	-54.796
0.3	-29.543	4.688	8.675	27.431	0.565	0.250	1.831	0.007	-53.128
0.35	-33.937	-0.171	5.047	24.055	0.421	0.317	2.259	0.007	-60.645
0.4	-38.055	1.218	5.236	27.000	0.428	0.244	1.806	0.007	-56.949
0.45	-41.790	3.289	5.590	30.388	0.453	0.163	1.306	0.006	-48.104
0.5	-45.033	3.724	5.156	32.365	0.438	0.129	1.094	0.006	-44.223
0.55	-47.651	3.228	4.431	33.705	0.403	0.121	1.042	0.006	-44.856
0.6	-49.488	3.229	3.988	35.528	0.382	0.106	0.936	0.006	-43.082
0.65	-50.372	4.223	3.925	38.081	0.383	0.073	0.706	0.006	-35.002
0.7	-50.129	5.474	3.945	40.809	0.389	0.038	0.459	0.006	-24.285
0.75	-49.008	5.853	3.723	42.985	0.378	0.024	0.342	0.006	-18.729
0.8	-47.035	5.150	3.251	44.552	0.347	0.032	0.368	0.006	-20.183
0.85	-44.292	4.874	2.945	46.453	0.326	0.032	0.348	0.006	-18.937
0.9	-38.892	7.385	3.336	49.938	0.356	-0.016	0.026	0.006	-1.344
0.9375	-33.163	10.980	4.014	53.581	0.402	-0.075	-0.360	0.006	17.216
0.975	-26.033	11.613	4.090	55.567	0.400	-0.084	-0.428	0.006	16.761
1	0.000	-39.532	-7.612	50.283	-0.628	0.936	5.881	0.018	0.000

Section 6 – Conclusions

The fundamental goal driving the motivation behind this thesis was to explore the similarities between performance estimates of propellers made by a program written in FORTRAN implementing a lifting line theory versus the published experimental data. The propellers tested include three Wageningen B-Series propellers, the geometry and performance characteristics of which may be found in Kuiper's 1992 publication *The Wageningen Propeller Series*. Open water charts are published with non-dimensional thrust, torque, and efficiency curves for each propeller in the last chapter. The lifting line theory program over predicts the thrust and torque, and some measures were taken to identify the location of the error. In particular, extra attention was paid to the various subroutines used to discretize the blade, compute the sectional circulation, calculate Fourier series coefficients, etc. Though numerous unnoticed errors were found and corrected, no satisfying solution was obtained which sufficiently improves the program. It is suspected that these errors are associated with the application of Glauert's solution (1947) for 2-D foils to the rotating marine propeller.

As previously mentioned, numerous other lifting line codes have been developed to analyze the performance characteristics of a propeller given its associated geometrical data. Two examples of these include the much-tested open-source OPENPROP which utilizes MATLAB (Epps, 2010) and a Master's thesis written by S. R. Kesler at the University of Utah. OPENPROP is known to produce reliable solutions which agree well with experimental data and is based on a Vortex Lattice formulation of lifting line theory. This is similar to planar lifting line theory, as implemented in this thesis, except the vortex system is assumed to be generated by a sequence of horseshoe elements rather than free vortex elements. This new approach to solving for the induced velocities could produce different results but likely will not remedy the bound circulation distribution errors.

Kesler (2014) wrote a lifting line code and conducted an experiment on a propeller in which he measured the thrust at various speeds. The results for produced thrust ranged from 36% in error to 195%, and the causes were identified as non-uniform propeller inflow, flow separation, and fluid compressibility. These errors are certainly significant considering the experimental setup and operation with a wooden airplane propeller, but none of these address the issue of unreasonably high thrust predicted with only the consideration of the bound circulation distribution.

OPENPROP utilizes an iterative optimization-based solution for finding the radial circulation distribution based on a number of parameters which are to be optimized, and Kesler develops a system of equations to be solved based on Prandtl's original formulation. It is possible that the error experienced with the subroutine implementing Glauert's solution is related to the assumption that the blade span is much larger than the chord length, which is certainly not true for marine propellers. Marine propellers have very low aspect ratios and significant tip vortices at high rates of revolution causing the pressure to equalize on the face and back of the blade very near the tip. This is the physical principle that motivates driving the sectional circulation to zero at $r/R = 1.0$.

Section 7 – Future Work

Several options may be considered for continuing to develop the program. Some comparison techniques may be incorporated to evaluate the efficiencies or torque requirements of more than one propeller. This could be valuable so as to reduce the time required for a user to select a propeller when performing an iterative analysis on different propeller characteristics. Also, the cavitation check in the perturbation velocity subroutines could be completed with the incorporation of the cavitation number. This would provide insight regarding the range of permissible operating conditions, efficiency, and noise produced.

Other further developments should certainly include a continuation of the literature review to determine why Glauert's solution over predicts the thrust and torque. As discussed in the Results section of this report the thrust and torque predictions based solely on the radial circulation distribution are too high to conclude that the method is reliable. Therefore, more investigation should be performed either to discover what assumptions are invalid with the current method of implementation or to find a new technique for computing the sectional bound vorticity and its effects on the local velocity distribution.

References

Birk, L. (2015). Program to generate B-Series propeller diagram. Python program, unpublished. Used to generate Figure 4.

Epps, B.P. (2010). An impulse framework for hydrodynamic force analysis: fish propulsion, water entry of spheres, and marine propellers. Massachusetts Institute of Technology. Dissertation.

Carlton, J.S. (2012). *Marine Propellers and Propulsion (3rd ed.).* City, State: Elsevier Ltd.

Kerwin, J.E., and Hadler, J.B. (2010). *The Principles of Naval Architecture Series: Propulsion*. Jersey City, NJ: SNAME.

Kesler, S.R. (2014). Propeller thrust analysis using Prandtl's lifting line theory. University of Utah. Master's thesis.

Kuiper, G. (1992). *The Wageningen Propeller Series*. Netherlands: MARIN.

Lerbs, H.W. (1952). Moderately Loaded Propellers with a Finite Number of Blades and an Arbitrary Distribution of Circulation. *Transactions*, vol. 60. New York, NY: SNAME.

Lewis, E.V. (ed). (1988). *Principles of Naval Architecture: Volume 2 Resistance, Propulsion, and Vibration*. Jersey City, NJ: SNAME.

Rao, G. Shanker. (2006). *Numerical Analysis (3rd ed.).* Daryagani, New Delhi: New Age International Publishers.

Wrench, J.W. (1957). The Calculation of Propeller Induction Factors: AML Problem 69-54, Technical Report 1116. David Taylor Model Basin, Department of the Navy, *Research and Development Report*. Alexandria, VA. http://www.dtic.mil/dtic/tr/fulltext/u2/224732.pdf. Accessed 14 Jan, 2016.

Additional Bibliography

Bertram, V. (2000). *Practical Ship Hydrodynamics*. City, State: Butterworth-Heinemann.

Breslin, J.P., & Anderson, P. (1994). *Hydrodynamics of Ship Propellers*. Cambridge, MA: Cambridge University Press.

Flood, K.M. (2008). Propeller performance analysis using lifting line theory. Massachusetts Institute of Technology. Master's thesis.

Glauert, H. (1947). *The Elements of Aerofoil and Airscrew Theory*. New York, NY: Cambridge University Press.

Newman, John N. (1977). *Marine Hydrodynamics*. Cambridge, MA: MIT Press.

Taravella, B.M. (2015). *Offshore Structure and Ship Dynamics*. NAME 3160 Lecture Notes, University of New Orleans.

Appendices

Appendix A: Program Instructions

After the source code for the program *liftline* is compiled, an executable file can be created which performs the calculations. The computations performed assume that the user has input data for the propeller diameter and speed of advance in English units. This is because standard values for the density and viscosity of seawater have been used. This could easily be adapted for metric units, if desired.

Appendix B: Sample Input File contains a sample input file demonstrating the required format. The number of decimal places on each number are irrelevant with the exception of the number of blades Z and the number of blade sections Ns which must be integers, i.e. they have no decimal. The program will display an error if the input file is improperly formatted. This requires that the quantity Ns (in sample file, Ns = 18) match the number of sections given. Otherwise, once again, an error message will display. In addition, the file name must be titled *input* and have a .txt extension.

The program can be executed once the input file, input.txt, has been transferred to the same folder in which the program is located. The program searches the current folder for the presence of the input file.

A logical flowchart is given for the user's convenience. The intent is to clarify the progression of the code so that it can be more easily understood by the unfamiliar user.

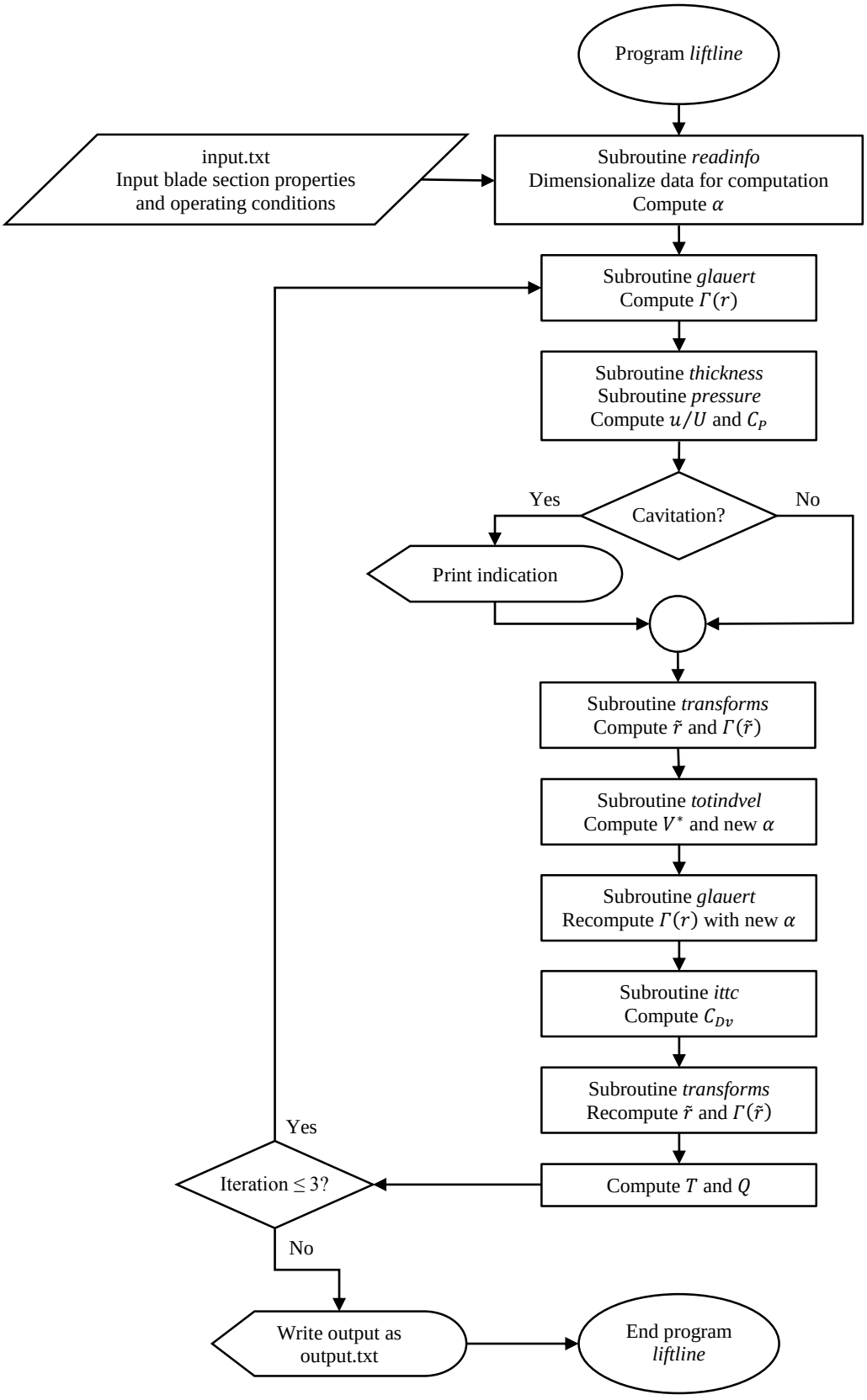
Program *liftline*
input.txt
Input blade section properties
and operating conditions
Subroutine *readinfo*
Dimensionalize data for computation
Compute α
Subroutine *glauert*
Compute $\Gamma(r)$
Subroutine *thickness*
Subroutine *pressure*
Compute u/U and C_P
Yes
Cavitation?
No
Print indication
Subroutine *transforms*
Compute $\tilde{r}$ and $\Gamma(\tilde{r})$
Subroutine *totindvel*
Compute V^* and new α
Subroutine *glauert*
Recompute $\Gamma(r)$ with new α
Subroutine *ittc*
Compute C_{Dv}
Subroutine *transforms*
Recompute $\tilde{r}$ and $\Gamma(\tilde{r})$
Compute T and Q
Yes
Iteration ≤ 3?
No
Write output as
output.txt
End program
liftline

Appendix B: Sample Input File

Below is the geometry and operating conditions used for Propeller 1, a B4-70 propeller. This demonstrates the appropriate formatting required for the program to know where each piece of information is going to be located when it is read. Note that sections r/R = 0.25, 0.35, 0.45, 0.55, 0.65, 0.75, 0.85, and 0.9375 resulted from interpolating the sections defined by the equations given for the geometry, and section r/R = 1.0 has linear dimensions that are set to ~zero.

```
5.330         ft propeller diameter
4             number of blades
183.0         RPM
20.0          ft/s advance velocity
21            chordwise discretization
18            number of blade sections
r/R           chord/rad     thick/chord   camber/chord  pitch/diam
0.2           0.56000000    0.130714286   0.02222143    1.150800
0.25          0.60239375    0.114856317   0.02263340    1.196650
0.3           0.64120000    0.101060512   0.02314286    1.241800
0.35          0.67641875    0.089326870   0.02374979    1.286250
0.4           0.70805000    0.079655392   0.02445421    1.330000
0.45          0.74382500    0.071050000   0.02508000    1.364738
0.5           0.75705000    0.063404002   0.02529820    1.388800
0.55          0.77402500    0.056581000   0.02499600    1.400000
0.6           0.78505000    0.050442647   0.02406114    1.400000
0.65          0.78876900    0.044838000   0.02237900    1.400000
0.7           0.78645000    0.039671944   0.01983597    1.400000
0.75          0.77371900    0.034920000   0.01742300    1.400000
0.8           0.74620000    0.030554811   0.01527741    1.400000
0.85          0.70958333    0.026367991   0.01318400    1.400000
0.9           0.62930000    0.022882568   0.01144128    1.400000
0.9375        0.54043125    0.020728793   0.01036440    1.400000
0.975         0.42700000    0.018969555   0.00948478    1.400000
1.0           0.00000001    0.016000000   0.00000001    1.400000
```

Appendix C: Open Water Diagrams Used

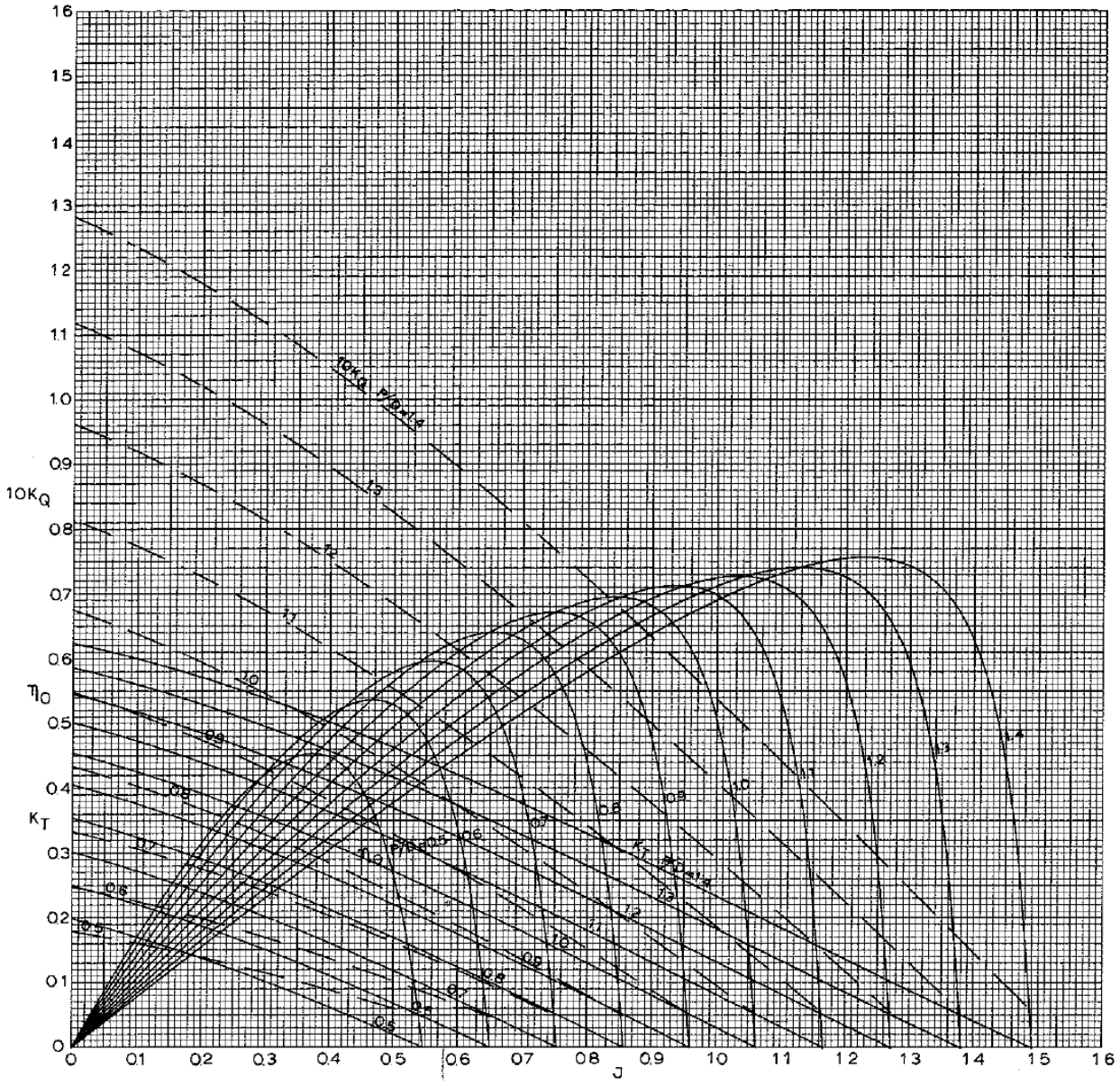

Figure 12: B4-70 open water diagram (Kuiper, 1992)

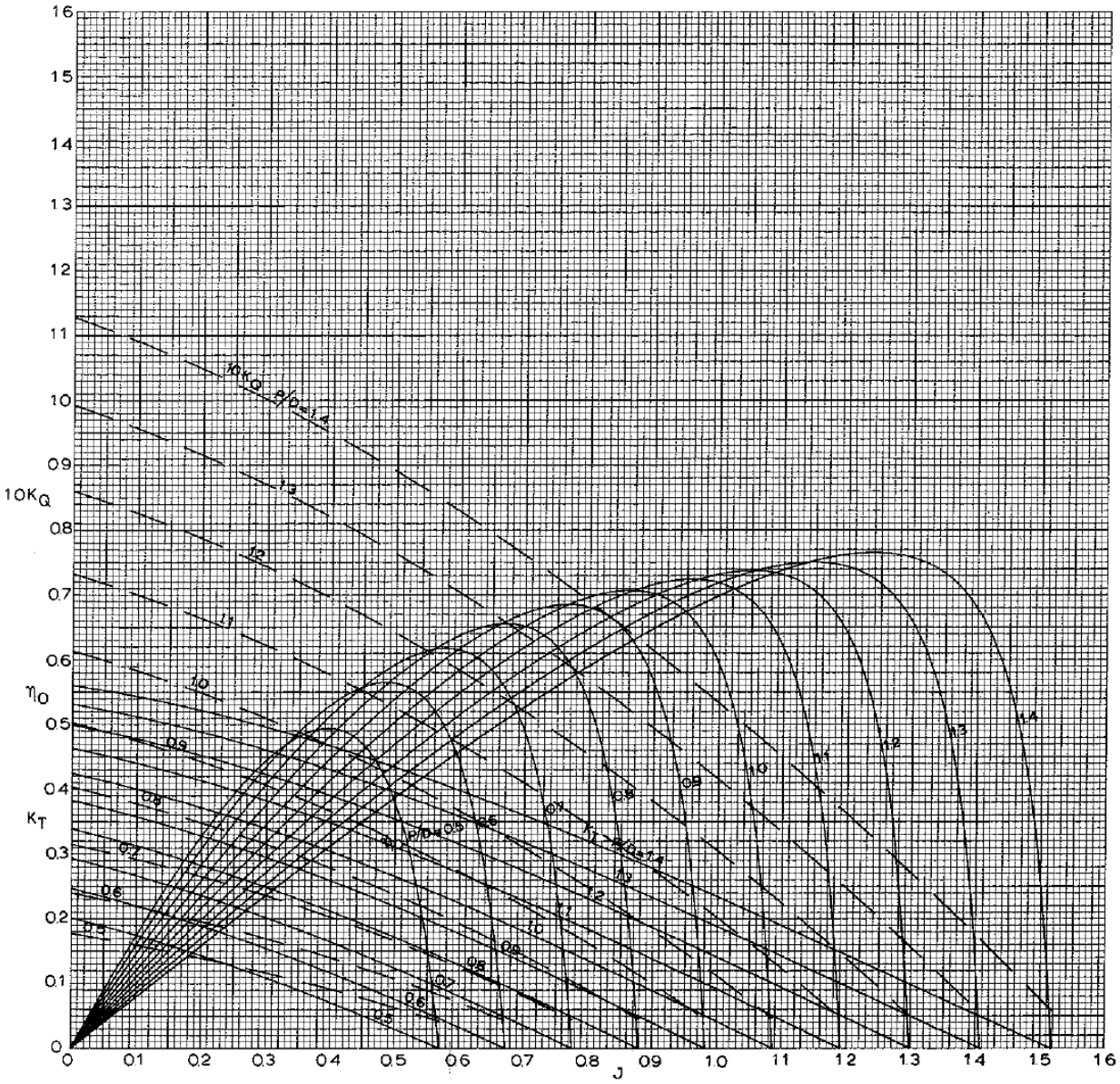

Figure 13: B4-55 open water diagram

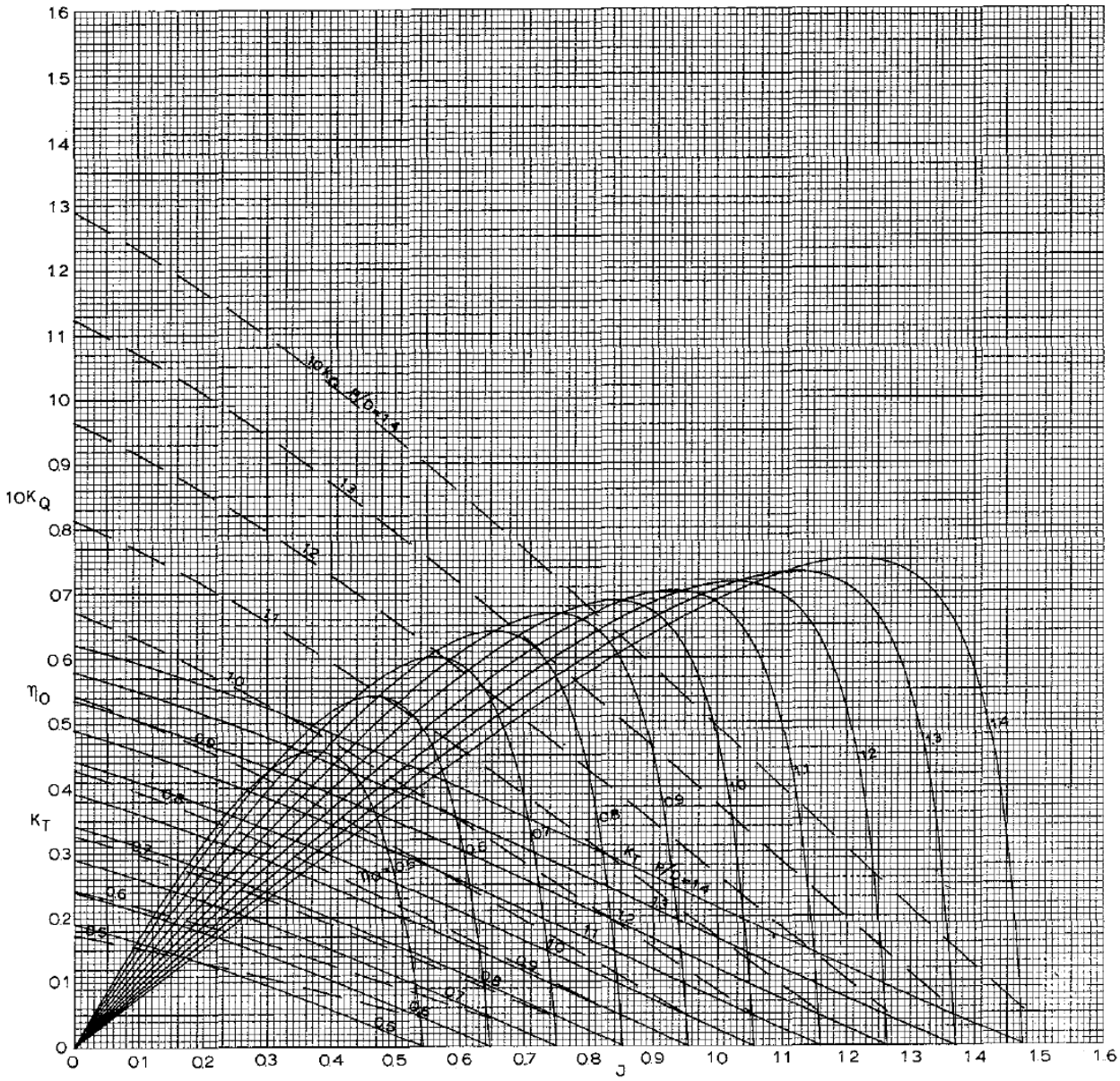

Figure 14: B3-65 open water diagram